Publications of the Korean Astronomical Society
**30**: 545 ∼ 548, 2015 September

pISSN: 1225-1534
eISSN: 2287-6936
http://dx.doi.org/10.5303/PKAS.2015.30.2.545

# PARTICLE ACCELERATION IN SUPERNOVA REMNANTS

Hyesung Kang
Department of Earth Sciences, Pusan National University, Pusan 609-735, Korea
*E-mail: hskang@pusan.ac.kr*
*(Received November 30, 2014; Reviced May 31, 2015; Aaccepted June 30, 2015)*

## ABSTRACT

Most high energy cosmic rays (CRs) are thought to be produced by diffusive shock acceleration (DSA) in supernova remnants (SNRs) within the Galaxy. Plasma and MHD simulations have shown that the self-excitation of MHD waves and amplification of magnetic fields via plasma instabilities are an integral part of DSA for *strong* collisionless shocks. In this study we explore how plasma processes such as plasma instabilities and wave-particle interactions can affect the energy spectra of CR protons and electrons, using time-dependent DSA simulations of SNR shocks. We demonstrate that the time-dependent evolution of the shock dynamics, the self-amplified magnetic fields and Alfvénic drift govern the highest energy end of the CR energy spectra. As a result, the spectral cutoffs in nonthermal X-ray and $\gamma$-ray radiation spectra are regulated by the evolution of the highest energy particles, which are injected at the early phase of SNRs. We also find that the maximum energy of CR protons can be boosted significantly only if the scale height of the magnetic field precursor is long enough to contain the diffusion lengths of the particles of interests. Thus, detailed understandings of nonlinear wave-particle interactions and time-dependent DSA simulations are crucial for understanding the nonthermal radiation from CR acceleration sources.

*Key words:* cosmic ray acceleration — shock wave — Supernova Remnants

## 1. INTRODUCTION

In collisionless shocks, suprathermal particles are scattered by MHD/plasma waves in the converging flow and accelerated to high energies through multiple crossings of the shock transition (Bell, 1978; Malkov & Drury, 2001). Supernova remnants (SNRs), strong powerful astrophysical shocks, are thought to produce most of the Galactic cosmic rays (CRs) up to $Z{\cdot}10^{15.5}$eV (where $Z$ is the charge number of CR nuclei) via the so-called diffusive shock acceleration (DSA)(Kang, 2010). Multi-band observations of nonthermal emission from radio to $\gamma$-ray can provide direct evidence for and a tool to examine the CR acceleration in SNRs. For instance, X-ray continua observed in thin rims of several young Galactic SNRs can be interpreted as synchrotron emission from $\sim 100$ TeV electrons cooling radiatively in a magnetic field of $\sim 100\mu$G, indicating effective magnetic field amplification (MFA) in strong SNR shocks (Caprioli, 2012).

CR protons streaming upstream in the shock precursor excite resonant Alfvén waves and amplify turbulent magnetic fields into the nonlinear regime (Bell, 1978; Lucek & Bell, 2000). In addition, the nonresonant fast-growing instability driven by the CR current upstream can amplify the magnetic field on scales shorter than proton gyro-scales by orders of magnitude (Bell, 2004; Riquelme & Spitkovsky, 2009). Then, the excited Alfvén waves drift with respect to the background flow with the drift speed, $u_w \approx +v_A$, where $v_A = B/\sqrt{4\pi\rho}$ is the local Alfvén speed (Bell, 1978). As the particles are isotropized in the mean wave frame, the resulting CR spectrum becomes much softer than predicted with the velocity jump for the background flow (Kang, 2012). Thus, self-consistent treatments of plasma instabilities and wave-particle interactions such as MFA and Alfvénic drift are important in understanding the nonlinear DSA at SNRs.

In this paper, we explore the effects of plasma processes by performing time-dependent DSA simulations with phenomenological models for MFA and Alfvénic drift.

## 2. DSA SIMULATIONS FOR SNRs

### 2.1. Spherical CRASH Code

We consider DSA of CR protons and electrons at gas dynamical shocks in a one-dimensional (1D) spherical geometry. We therefore solve the following time-dependent diffusion-convection equation for the pitch-angle-averaged phase space distribution function for CR particles, $g(r,p,t) = f(r,p,t)p^4$ (Skilling, 1975):

$$\frac{\partial g}{\partial t} + (u+u_w)\frac{\partial g}{\partial r} = \frac{1}{3r^2}\frac{\partial}{\partial r}\left[r^2(u+u_w)\right]\left(\frac{\partial g}{\partial y} - 4g\right) + \frac{1}{r^2}\frac{\partial}{\partial r}\left[r^2\kappa(r,y)\frac{\partial g}{\partial r}\right] + p\frac{\partial}{\partial y}\left(\frac{b}{p^2}g\right), \quad (1)$$

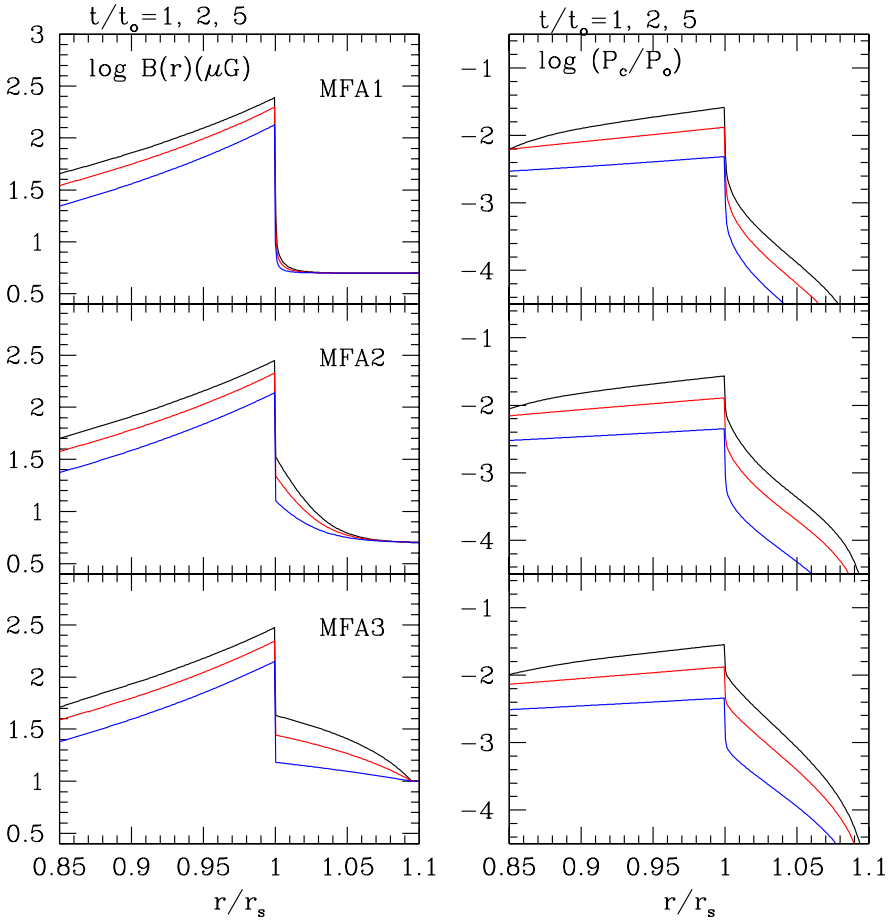


Figure 1. Time-dependent DSA simulation results of a model SNR with three magnetic field amplification models, **MFA1**, **MFA2**, and **MFA3**, at $t/t_{\rm o} = 1$ (black solid lines), 2 (red), and 5 (blue). Left: magnetic field profiles. Right: CR pressure profiles.

where $u$ and $u_w$ are the flow velocity and wave drift velocity, respectively, $y = \ln(p/m_{\rm p}c)$, and $\kappa(r,p)$ is the spatial diffusion coefficient. The term $b(p) = -dp/dt$ accounts for electron synchrotron and inverse-Compton losses (Kang et al., 2013).

In order to examine the maximum effects of the Alfvénic drfit, we adopt $u_{w,2} = -v_{A,2}$ behind the shocks and $u_{w,1} = +v_{A,1}$ upstream of the shock. Hereafter we use the subscripts '0', '1', and '2' to denote conditions far upstream of the shock, immediately upstream and downstream of the subshock, respectively. The basic gasdynamic conservation laws with additional terms for the CR pressure are solved using the spherical version of the CRASH (Cosmic-Ray Amr SHock) code (Kang & Jones, 2006). The CR pressure is calculated self-consistently from the CR proton distribution function, $g_{\rm p}(p)$, determined from equation (1). The magnetic pressure is calculated according to our phenomenological models for MFA described in Section 2.2. In addition, we assume that Bohm diffusion is valid because of resonant scattering with self-excited waves, i.e., $\kappa(p) = (1/3)r_g(p)v$.

### 2.2. *Magnetic Field Amplification Model*

Here we consider three heuristic models for MFA in the precursor designated **MFA1** - **MFA3**, and compare their consequences in DSA.

**MFA1** model: MFA factor increases with $M_A^2$ and the degree of the compression in the precursor as

$$\frac{B(r)^2}{B_0^2} = 1 + \frac{4}{25} M_{\rm A,0}^2 \frac{(1-U(r)^{5/4})^2}{U(r)^{3/2}}, \qquad (2)$$

where $U(r) = [u_{\rm s} - |u(r)|]/u_{\rm s}$ is the normalized flow speed in the precursor and $M_{\rm A,0} = u_{\rm s}(t)/v_{\rm A,0}$ is the Alfvénic Mach number in the far upstream flow.

**MFA2** model: The magnetic field strength decreases exponentially with a scale height $L$ in the precursor as

$$B(r) = B_0 + B_1 \cdot (\frac{B_1}{\delta B_0})^{-(r-r_{\rm s})/L}, \qquad (3)$$

where $\delta B_0$ is an arbitrary strength of the initial background magnetic field perturbations and $B_1$ is the immediate preshock magnetic field strength determined by Eq. (2).

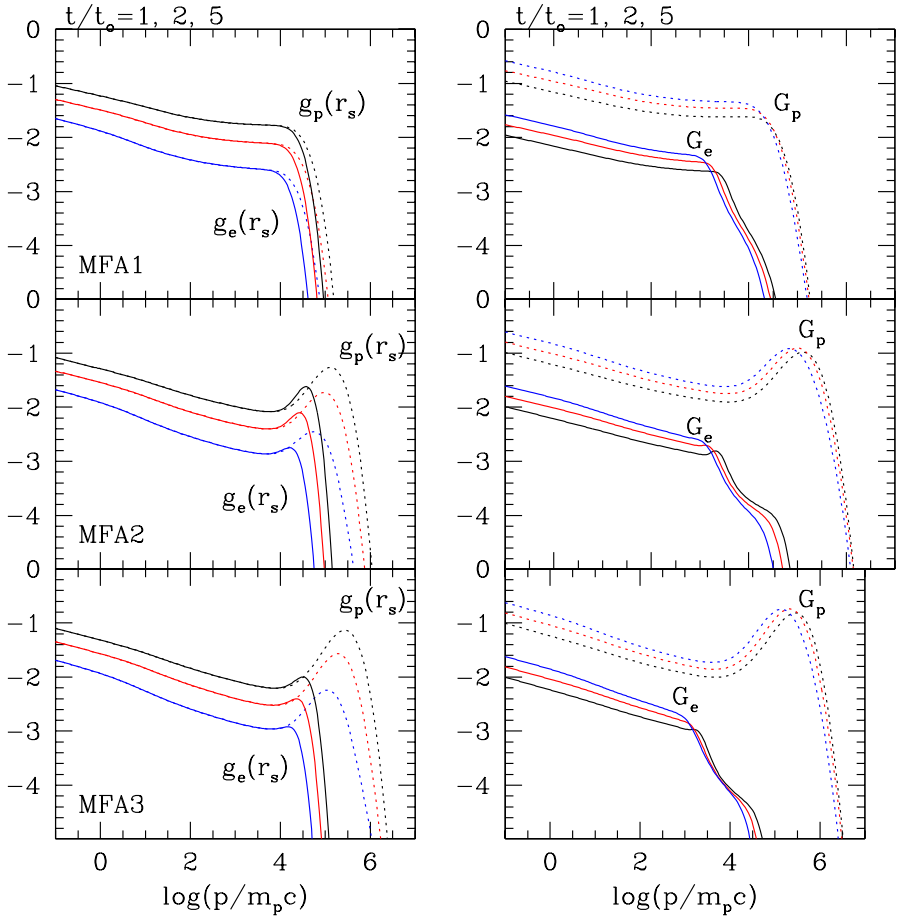


Figure 2. Time-dependent DSA simulation results of a model SNR with three magnetic field amplification models, **MFA1**, **MFA2**, and **MFA3**, at $t/t_{\rm o} = 1$ (black), 2 (red), and 5 (blue). Left: Energy spectrum at the shock location, $g_p(r_s)$ for protons (dotted lines), and $g_e(r_s)$ for electrons (solid lines). Right: Volume integrated energy spectrum, $G_p(p) = \int 4\pi g_p(p) r^2 dr$ for protons (dotted lines), and $G_e(p) = \int 4\pi g_e(p) r^2 dr$ for electrons (solid lines). For clarity of the plot, we adopt $K_{e/p} = 0.1$ for $G_e$here.

**MFA3** model: The magnetic field strength decreases linearly with a scale height $L$ in the precursor as

$$B(r) = B_1 - (B_1 - B_0) \cdot \frac{r - r_{\rm s}}{L}. \qquad (4)$$

In the downstream of the shock, we assume the magnetic field strength scales with the gas density as $B(r) = B_2(\rho(r)/\rho_2)$, where $B_2/B_1 = \sqrt{1/3 + 2/3(\rho_2/\rho_1)^2}$ is the immediate postshock magnetic field strength, which is amplified through the shock compression. The left panels of Fig. 1 show how the profiles of $B(r,t)$ evolves in the three models.

### 2.3. *Supernova Remnant Model Parameters*

We consider a Type Ia supernova explosion with the ejecta mass, $M_{\rm ej} = 1.4 M_{\rm sun}$, and the explosion energy, $E_{\rm o} = 10^{51}$ ergs that expands into a warm uniform ISM with $n_{\rm H} = 0.3{\rm cm}^{-3}$ and $T_0 = 3 \times 10^4$K. The sonic Mach number of the blast wave is $M_s \approx 115(u_{\rm s}/3000 \text{ km s}^{-1})$, so the compression ratio is $\sigma = 4$. The background magnetic field strength is set to be $B_0 = 5$ $\mu$G, so the upstream Alfvén speed is $v_{\rm A,0} = 16.8$ km s$^{-1}$. The associated shock Alfvén Mach number is $M_{\rm A,0} \approx 180(u_{\rm s}/3000 \text{ km s}^{-1})$, so the MFA factor is expected to be quite high.

We start each simulation from the Sedov-Taylor similarity solution for the forward shock only: $r_s/r_{\rm o} = 1.15(t/t_{\rm o})^{2/5}$ and $u_s/u_{\rm o} = 0.46(t/t_{\rm o})^{-3/5}$, where $r_{\rm o} = (3M_{\rm ej}/4\pi\rho_{\rm o})^{1/3}$=3.18pc, $t_{\rm o} = \left(\rho_{\rm o} r_{\rm o}^5/E_{\rm o}\right)^{1/2}$=255 years, and $u_{\rm o} = r_{\rm o}/t_{\rm o} = 1.22 \times 10^4$ km s$^{-1}$ are normalization constants.

We adopt a thermal leakage model for CR injection in which suprathermal particles with $p \geq p_{\rm inj}(t) \approx 7.4 m_p u_s(t)/\sigma$ are allowed to cross the shock and participate in the DSA process (Kang et al., 2002). Since thermal electrons have much smaller rigidities at a given energy, electrons are expected to be injected with a much smaller injection rate than protons (Kang et al., 2014). However, we simply assume that the electrons are injected with $K_{e/p} = 1$ in the simulations, since we are

not interested in the relative ratio of the two populations here. Our primary objective here is to examine the effects of MFA and Alfvénic drift on the DSA process.

## 3. RESULTS AND DISCUSSION

The left panels of Fig. 1 show how the magnetic field profile evolves in time in the three adopted MFA models. As seen in the figure, the downstream magnetic field strength ranges from $B_2 \sim 200 - 300$ $\mu$G and decreases overall in time as the shock slows down. As noted in the Introduction, this is consistent with the postshock magnetic fields inferred from X-ray observations of young SNRs (Caprioli, 2012). The right panels of Fig. 1 show the spatial profiles of the CR pressure, $P_{CR}$. In the MFA3 model, in which the MFA profile is the broadest among the three, the precursor width of $P_{CR}$ is also the most substantial and so the CR energy generation is the greatest.

In the left panels of Fig. 2 the energy spectra at the shock location, $g_p(r_s)$ for protons and $g_e(r_s)$ for electrons are plotted. Note that here $K_{e/p} = 1$, so the only difference between protons and electrons is the radiative cooling of electrons. So the electron energy spectra could cutoff at lower energies due to cooling, compared to the proton energy spectra.

In the model with the *broader* MFA precursor, the maximum energy (or cutoff energy) of the proton energy spectrum becomes higher, so $p_{\rm max,p} \approx 10^{13}{\rm eV}/c$ in the **MFA1** model, while $p_{\rm max,p} \approx 10^{15}{\rm eV}/c$ in the **MFA3** model. So the width of the MFA precursor should be broad enough to contain PeV protons in order to boost CR proton energies up to the knee energy of $10^{15.5}$ eV via MFA in the upstream of SNR shocks. On the other hand, the electron cutoff energy, $p_{\rm max,e} \approx 10^{13}{\rm eV}/c$, is similar in all three models, because $p_{\rm max,e}$ is mainly controlled by radiative cooling behind the shock. As a result, in the **MFA3** model, the difference between $p_{\rm max,p}$ and $p_{\rm max,e}$ is the greatest. The power-law slope for both $g_p(r_s)$ and $g_e(r_s)$ below $p < 10^3 m_p c$ is $q \approx 4.2$, so the energy spectrum is $N(E) \propto E^{-2.2}$ for low energy CRs. For the high energy end ($p > 10^3 m_p c$), however, the CR spectra have nonlinear curvatures and depend sensitively on the details of MFA models.

The right panels of Fig. 2 show the volume integrated energy spectrum, $G_p(p) = \int 4\pi g_p(p) r^2 dr$ for protons, and $G_e(p) = \int 4\pi g_e(p) r^2 dr$ for electrons at the three epochs, $t/t_{\rm o} = 1$, 2, and 5. Postshock electrons cool radiatively while advecting downstream, so the electron spectrum cuts off at a progressively lower momentum away from the shock. As a result, the volume integrated electron energy spectrum, $G_e(p)$, becomes steeper than the proton energy spectrum, $G_e(p)$, by one power of the momentum for $p > p_{\rm e,br}$, where the break momentum is $p_{\rm e,br} \approx 10^{12}{\rm eV}/c$ in these models.

Since the high energy end of the CR proton spectrum consists of the particles that are injected during the early stages of SNRs, the spectral shape near the high energy cutoff is governed by the time-dependent evolution of the shock dynamics, the CR injection and the MFA. So the ensuing $\pi^0$ decay $\gamma$-ray emission would differ as well, depending on these time-dependences. But the electron spectrum depends much less sensitively on the evolution of those quantities, since it is more or less in instantaneous equilibrium with local values due to short radiative cooling time scales. This study demonstrates that a detailed understanding of plasma physical processes operating at collisionless shocks is crucial in predicting the CR energy spectra accelerated at SNR shocks and nonthermal emissions due to those CRs.

## ACKNOWLEDGMENTS

This work was supported by the National Research Foundation of Korea Grant funded by the Korean Government (NRF-2012R1A1B3001065).

## REFERENCES

Bell, A. R., 1978, The Acceleration of Cosmic Rays in Shock Fronts. I, MNRAS, 182, 147

Bell, A. R., 2004, Turbulent Amplification of Magnetic Field and Diffusive Shock Acceleration of Cosmic Rays, MNRAS, 353, 550

Caprioli, D., 2012, Cosmic-Ray Acceleration in Supernova Remnants: Non-Linear Theory Revised, JCAP, 7, 38

Kang, H., 2010, Cosmic Ray Spectrum in Supernova Remnant Shocks, JKAS, 43, 25

Kang, H., 2012, Diffusive Shock Acceleration with Magnetic Field Amplification and Alfvénic Drift, JKAS, 45, 127

Kang, H., 2013, Effects of Wave-Particle Interactions on Diffusive Shock Acceleration at Supernova Remnants, JKAS, 46, 49

Kang, H. & Jones, T. W., 2006, Numerical Studies of Diffusive Shock Acceleration at Spherical Shocks, APh, 25, 246

Kang, H., Jones, T. W., & Edmon, P. P., 2013, Nonthermal Radiation from Supernova Remnants: Effects of Magnetic Field Amplification and Particle Escape, ApJ, 777, 25

Kang, H., Jones, T. W., & Gieseler, U. D. J., 2002, Numerical Studies of Cosmic-Ray Injection and Acceleration, ApJ, 579, 337

Kang, H., Vahe, P., Ryu, D., & Jones, T. W., 2014, Injection of $\kappa$-like Suprathermal Particles into Diffusive Shock Acceleration, ApJ, 788, 141

Lucek, S. G. & Bell, A. R., 2000, Non-linear Amplification of a Magnetic Field Driven by Cosmic Ray Streaming, MNRAS, 314, 65

Malkov M. A. & Drury, L.O'C., 2001, Nonlinear Theory of Diffusive Acceleration of Particles by Shock Waves, RPPh, 64, 429

Riquelme, M. A. & Spitkovsky, A., 2009, Nonlinear Study of Bell's Cosmic Ray Current-Driven Instability, ApJ, 694, 626

Skilling, J., 1975, Cosmic Ray Streaming. I - Effect of Alfvén Waves on Particles, MNRAS, 172, 557